Dalton Transactions

Accepted Manuscript

ROYAL SOCIETY OF CHEMISTRY

www.rsc.org/dalton

Unusual Non-bifunctional Mechanism for Co-PNP Complex Catalyzed Transfer Hydrogenation Governed by the Electronic Configuration of Metal Center

Cheng Hou, Jingxing Jiang, Yinwu Li, Zhihan Zhang, Cunyuan Zhao*, and Zhuofeng Ke*

MOE Key Laboratory of Bioinorganic and Synthetic Chemistry/KLGHEI of Environment and Energy Chemistry, School of Chemistry and Chemical Engineering, Sun Yat-sen University, Guangzhou 510275, P. R. China

ABSTRACT

The mimic of hydrogenases has unleashed a rising tide of bifunctional catalysts, which are widely used in the catalytic hydrogenation of polar multiple bonds. With the ancillary ligand, the bifunctional mechanism is generally considered to proceed via the metal-ligand cooperation transition state. Inspired by the interesting work performed by Hanson et al. (*Chem Commun*. 2013, 49, 10151), we present a computational study of a distinctive example that Co^{II}-PNP catalyst with the ancillary ligand achieves efficient transfer hydrogenation through a non-bifunctional mechanism. Both bifunctional and non-bifunctional mechanisms are discussed. The calculated results based on the full model of the catalyst suggest that the inner-sphere non-bifunctional mechanism is more favorable (by ~11 kcal/mol) than the outer-sphere bifunctional mechanism, which is in agreement with the experimental observations. This origin of mechanistic preference of Co^{II}-PNP catalyst can be attributed to the favor of square planar geometry. A traditional bifunctional mechanism is less plausible for Co^{II}-PNP due to the high distortion energy caused by the change of electronic configuration with the varied ligand field. Considering previous studies focusing on the development of ligands more often, this computational study indicates that the catalytic hydrogenation mechanism is not only controlled by the structure of ligand but also the electronic configuration of metal center.

INTRODUCTION

Catalytic hydrogenation is crucial for chemical hydrogen storage, and also has important applications in the fields of pesticide, pharmaceuticals and fine chemical synthesis.[1] Using different hydrogen sources, such as H_2, formate or alcohol, the hydrogenation reaction can occur through different mechanisms with the aid of transition metal (TM) catalyst. A general strategy to catalyze hydrogenation is to imitate the enzymatic hydrogenation, of which crucial residues serve as assisting ligands.[2-4] Various bio-inspired catalysts with ligands bearing a pendent base have been developed in the past few decades.[5-7] These catalysts are usually regarded as "bifunctional" catalyst,[8] due to the metal-ligand cooperation during hydrogenation, that is, the protonated pendent base transfers proton meanwhile the metal center transfers the hydride to the substrate in an outer-sphere manner (Figure 1).[9] On the other hand, the alternative non-bifunctional pathway through the inner-sphere will proceed without the participation of the ancillary pendent base.

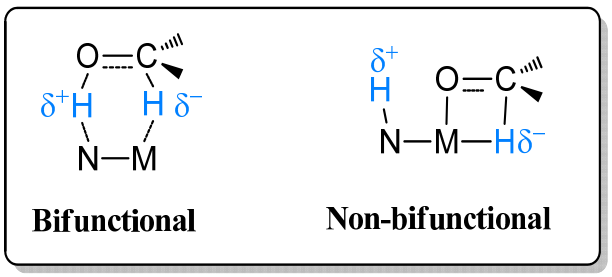

Figure 1. The typical bifunctional and non-bifunctional mechanisms.

An early example for the bifunctional hydrogenation catalysts, is Shvo's ruthenium hydride complex (RuH(Ph$_4$(η^5-C$_4$COH)) (Figure 2A) reported in the early 1980s.[10-14] A recent mechanistic study indicates the outer-sphere transition state is ~25 kcal/mol lower than the inner-sphere one. Before long, using chiral diamine and bisphosphine ligands, Noyori et al developed two ruthenium catalysts (Figure 2B and 2C),[15-17] which showed high activity and enantioselectivity with the chiral ancillary ligand bearing amine as assisting base. The mechanism was also verified to be an outer-sphere bifunctional process[18-20].

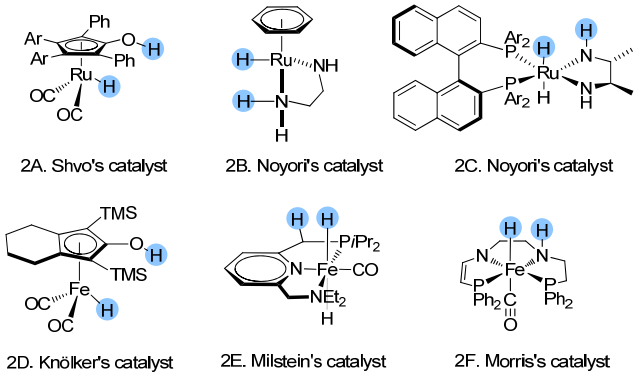

Figure 2. Examples of well-known bifunctional catalysts.

Later, more interests were attracted to develop catalysts with the first row earth-abundant metals such as Co and Fe to avoid using noble metals such as Ir[21-23], Rh[24,25] and Ru[26-28], due to the economical and environmentally benign desires. Casey et al performed several mechanistic studies on hydrogenation reactions catalyzed by the Knölker's catalyst,[29,30] suggesting the bifunctional concerted transfer on the outer-sphere[31,32]. The iron-PNN catalyst (Figure 2E) reported by Milstein et al. can catalyze the direct acylation of amines by alcohols and catalytic hydrogenation of ketone efficiently.[33] In the original paper, they proposed an inner-sphere mechanism which involved a ligand rotation to provide a vacant site. Later, the mechanism is verified to proceed a metal-ligand cooperation mechanism, through a unique aromatization-dearomatization mode[34-37]. Another 5,5,5-PNNP iron catalyst (Figure 2F) developed by Morris et al also performed high efficiency and enatioselectivity in transfer hydrogenation of ketone.[38-42] The amido and enamido ligands are suggested to assist the hydrogenation though a stepwise bifunction-al outer-sphere mode. With detailed computational and experimental kinetic investigations, they were able to further optimize the ligand structure and avoid the activation period of the catalyst.[43-47]

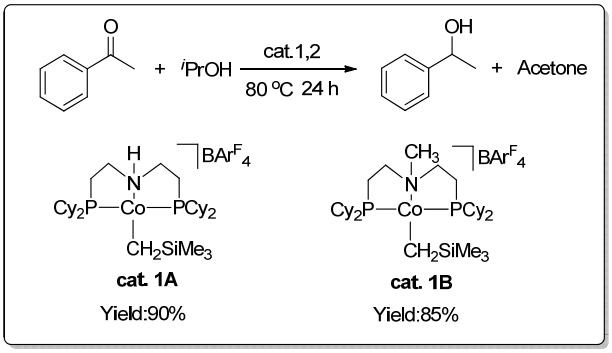

Scheme 1. The cobalt hydrogenation catalysts with PNP–NH (cat. 1A) and PNP–NMe (cat. 1B) as ligands.

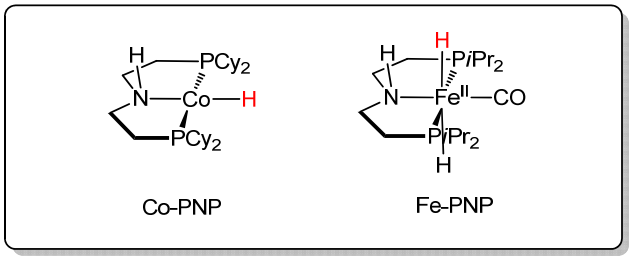

Figure 3. The Co-PNP catalyst (cat. 1A) after activated by hydrogen source and the Fe-PNP (cat. 2) catalyst

Former experimental and computational mechanism studies suggested that, "bifunctional" catalysts with ligands bearing pendent base should inclusively operates via the outer-sphere mechanism involving the metal-ligand cooperation. However, very recently, Hanson et al developed the Co^{II}-PNP pincer catalysts.[48-50] With an earth-abundant metal center, this catalyst is effective in transfer hydrogenation of C=O and C=N bonds. Especially, a unique phenomenon of interest is that, both two catalysts with N-H (cat. 1A in Scheme 1) and N-CH3 (cat. 1B in Scheme 1) are able to catalyze the transfer hydrogenation of acetophenone. It should be noted that this phenomenon is quite different from previous observation, which indicates that the pendent N-H moiety is not necessary for catalytic hydrogenation.[51] This interesting phenomenon becomes a sharp contrast to the Fe-PNP catalyst (Figure 3) developed by Guan and Beller separately, which prefer the outer-sphere mechanism bearing the similar ligand.[52-54] Yet the origin of this innocence is still not clear. Inspired by the interesting discovery made by Hanson et al, some

questions naturally arose. Is the bifunctional manner essential in this system? How does the catalytic hydrogenation operate without the metal-ligand cooperation? What is the inner difference between Co-PNP catalyst and Fe-PNP catalyst? With these questions in mind, we present a mechanistic study on the cobalt catalyzed hydrogenation of ketone. This study is expected to provide a deep insight into the unique mechanism of the distinctive cobalt catalyst, which are revelatory for the development of earth-abundant transition metal catalyst for hydrogenation in a convenient way without introducing pendent base on the ligand.

RESULTS

Inner-sphere stepwise transfer hydrogenation. Before the catalysis cycle begin, the pre-catalyst $[(PNHP^{Cy})Co(CH_2SiMe_3)]BAr^F_4$ will be activated to form a square planar metal hydride complex with the aid of hydrogen source, isopropyl alcohol, releasing one molecule of TMS (tetramethylsilane), which has been verified by former experimental study[48]. No matter what hydrogen source is used, the metal hydride should be the starting material of the catalytic hydrogenation process. Herein, focusing on the major catalytic cycle, we choose this metal hydride **1** complex as the starting point. As for the nomenclature, all the key intermediates and transition states are classified into **I-x** and **O-x**, in which x designates the number of intermediate. **I** and **O** designate the inner-sphere non-bifunctional mechanism and the outer-sphere bifunctional mechanism respectively. The initial metal hydride complex **1**, which stays at a square planar geometry, is able to isomerize to a square-based pyramidal (SBP) geometry as the PNP ligand is not rigid. Therefore, we will take both square planar geometry and square-based pyramidal geometry into our discussion.

As for the inner-sphere, the catalytic hydrogenation process occurs stepwise. It consists of three major step, the hydride transfer, the proton transfer and the hydride regeneration. The calculated result of the key intermediates and transition states of the hydride transfer step is presented in Scheme 2. For the square planar pathway, the acetophenone (AcPh) will coordinate to the metal center to form intermedi-

ate ***cis*-I-1** (ΔG = 6.6 kcal/mol). An isomer, ***trans*-I-1**, which has the AcPh coordinated to metal center *trans* to the N-H moiety, is calculated to be slightly less favored (ΔG = 7.5 kcal/mol). After the coordination, the hydride will transfer to the carbonyl of the substrate, AcPh, through the transition state ***cis*-I-TS1**, with an activation free energy of 29.5 kcal/mol. Another isomer for this inner-sphere hydride transfer transition sate, ***trans*-I-TS1**, is also studied. ***trans*-I-TS1** is 2.2 kcal/mol higher in free energy than ***cis*-I-TS1**. This can be attributed to the weak interaction between the N-H moiety and the carbonyl group (***cis*-I-TS1**: r(O...H^2) = 2.407Å), which will make the carbonyl more electrophilic and stabilize the transition state. With respect to the SBP pathway, the ***cis*-I-1** is able to isomerize to **I-1$_{bent}$**. The free energy of this isomerization is uphill for 12.8 kcal/mol. However, it is interesting that the hydride transfer step with the SBP geometry (**I-TS1$_{bent}$**: $\Delta G^{\ddagger}$ = 23.0 kcal/mol) is lower compared with ***cis*-I-TS1** (***cis*-I-TS1**: $\Delta G^{\ddagger}$ = 29.5 kcal/mol). It is mainly attributed to the differences of the nucleophilicity of metal hydride and the steric effects between these two transition states.

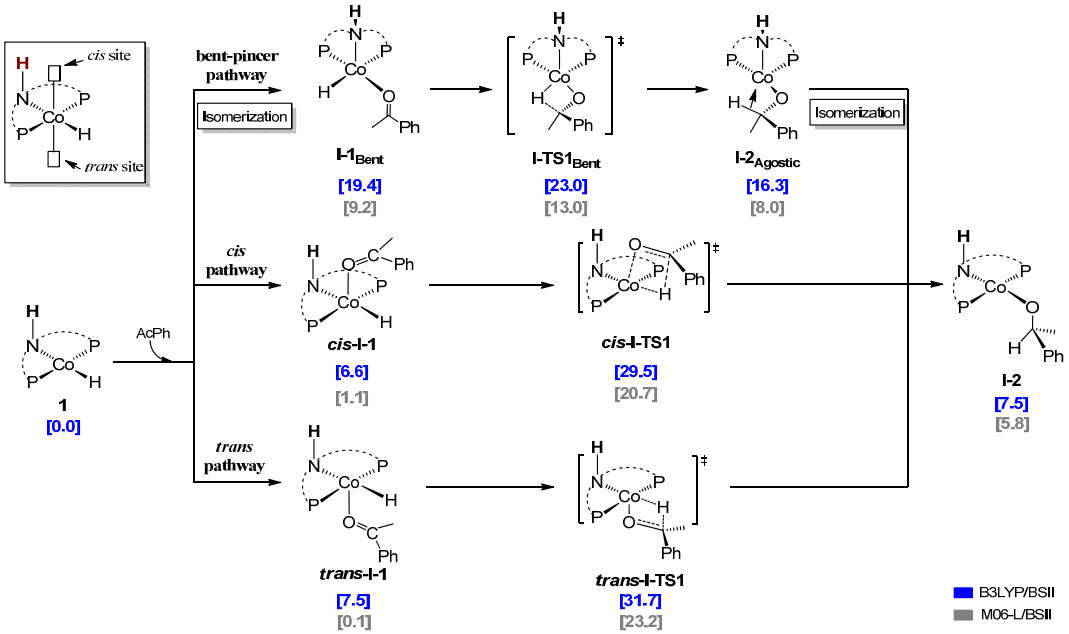

Scheme 2. The hydride transfer step of inner-sphere non-bifunctional mechanism. The relative free energies are given in kcal/mol.

After the hydride transfer step, a proton transfer to the benzyloxide complex **I-2** will occur to produce 1-phenylethanol. One possible pathway is to transfer the proton from IPA to benzyloxide to generate the 1-phenylethanol as product and the isopropoxide complex **I-4** for further reaction. Different processes are summarized in Figure 4. The direct transfer ***cis*-I-TS2** has an activation free energy of 27.9 kcal/mol. The proton transfer can also proceed *trans* to N-H moiety via ***trans*-I-TS2** ($\Delta G^{\ddagger}$ = 34.3 kcal/mol). Consistent with former proton transfer process, the abstraction of proton from isopropanol can also involve another molecule of isopropanol to form the "proton shuttle" type[53,55,56] transition state ***cis*-I-TS2$_{shuttle}$** or ***trans*-I-TS2$_{shuttle}$**. From Figure 4, we can see the proton transfer transition states ***cis*-I-TS2** and ***trans*-I-TS2** without proton shuttle are more difficult ($\Delta G^{\ddagger}$ = 27.9 and $\Delta G^{\ddagger}$ = 34.3 kcal/mol, respectively). As comparison, transition states ***cis*-I-TS2$_{shuttle}$** and ***trans*-I-TS2$_{shuttle}$** with "proton shuttle" will overcome relatively lower activation free energy ($\Delta G^{\ddagger}$ = 27.6 kcal/mol and 31.9 kcal/mol, respectively). The deviation between B3LYP/BSII and M06-L/BSII data is somehow large. It should be noted that the entropy penalty for a multiple component reaction can be offset by the dispersion stabilization in M06-L. This is further supported by the result of B3LYP-D3 functional, which leads to a relative energy of 9.8 kcal/mol for **cis-I-TS2**, similar to the result of M06-L (please see page S16, Support Information). After the proton transfer, the deprotonated isopropanol will form another metal isopropoxide complex **I-4**, which will regenerate the hydride in the next step.

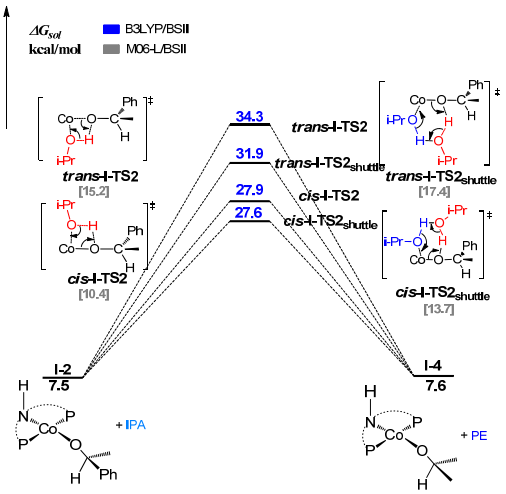

Figure 4. The free energy profiles of the proton transfer step via **I-TS2**. The PNP ligand in the transition state structures was removed for clearity. The relative free energies are given in kcal/mol.

An alternative pathway is to donate the proton of the N-H moiety to the benzyloxide (see Scheme 3). In this pathway, complex **I-2** goes through transition state **I-TS3** or **I-TS3$_{shuttle}$** to generate an amido complex **I-3** and 1-phenylethanol as product. The transition state **I-TS3** with an activation free energy of 32.0 kcal/mol indicates the proton on the N-H moiety is difficult to directly transfer to the metal alkoxide. In addition, the "proton shuttle" transition state **I-TS3$_{shuttle}$** using an isopropanol as a "proton bridge" can release the ring strain and lower the activation free energy by 1.3 kcal/mol. The non-saturated amido complex **I-3** is an energetically high intermediate (24.8 kcal/mol) in the potential energy surface. In order to regenerate the catalyst, the hydrogen source, IPA, has to transfer the proton and the hydride to the amido complex via a stepwise mechanism. The regeneration process is similar to the inverse process of former hydrogenation. The intermediate **I-3** can abstract the proton of IPA to produce the isopropoxide complex **I-4** via **I-TS4** or **I-TS4$_{shuttle}$**. The results suggest the "proton shuttle" mechanism (**I-TS4$_{shuttle}$**, $\Delta G^{\ddagger}$ = 28.1 kcal/mol) is more favored than the direct cleavage (**I-TS4**, $\Delta G^{\ddagger}$ = 31.9 kcal/mol). After then, the isopropoxide complex **I-4** is generated (7.6 kcal/mol). Another proton transfer (**I-TS5**) pathway via the isomer **I-2$_{vacant}$** bearing a bent PNP backbone is located with the energy barrier of 29.2 kcal/mol. The proton shuttle type, **I-TS5 $_{shuttle}$** ($\Delta G^{\ddagger}$ = 28.0 kcal/mol) is found to be slightly lower than **I-TS5**. The proton transfer from isopropanol (**I-2 → I-TS2 →I-4** or **I-2 → I-TS5 →I-4**) has relatively lower activation free energy than the proton transfer from N-H moiety does (**I-2 → I-TS3 → I-TS4 →I-4**). On the other hand, the difference in free energy between ***cis*-I-TS2$_{shuttle}$** and **I-TS5 $_{shuttle}$** is very tiny (~0.4 kcal/mol). Our calculated results suggest that both these two transfer modes are plausible. For further comparison of mechanistic preference, we consider that the proton transfer mechanism will proceed via the TS with the lowest energy barrier (***cis*-I-TS2 $_{shuttle}$**).

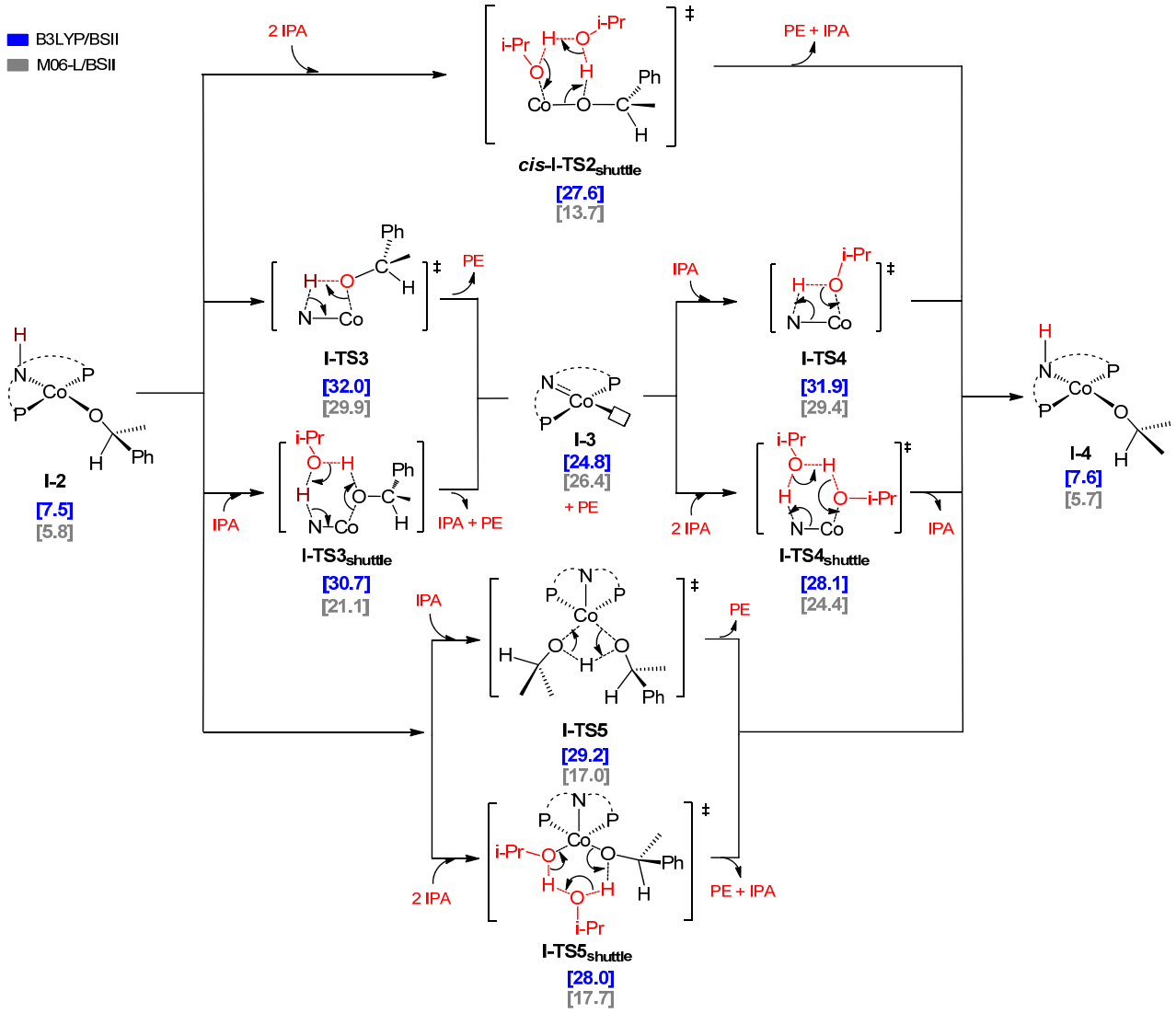

Scheme 3. The proton transfer step of inner-sphere non-bifunctional mechanism. The PNP ligand in the transition state structures was removed for clearity (PE is short for phenyl ethanol and IPA is short for isopropyl alcohol). The relative free energies are given in kcal/mol.

The final step of non-bifunctional hydrogenation mechanism is the *β*-hydride elimination from iso-propoxide complex **I-4** (see Scheme 4). **I-4** is also able to isomerize to SBP geometry, which provide two possible directions for *β*-hydride elimination. An important issue has to be clarified is that five co-ordinated status is saturated for d^7 metal as the six-coordinated Co^{II} species will lead to the unreasonable 19e electronic configuration (please see page S7 in Supporting Information, Figure S5). If the *β*-hydride elimination operates towards coordination site 2, it will lead to ***cis*-I-TS6**, in which the backbone of the

PNP ligand will turn into a non-bent geometry. The activation free energy of this ***cis*-I-TS6** is calculated to be 28.5 kcal/mol. The β-elimination transition state ***cis*-I-TS6** (acetone *cis* to N-H moiety) is 2.4 kcal/mol lower ***trans*-I-TS6** (acetone *trans* to N-H moiety), which is also consistent with former site preference for the carbonyl insertion step. If the hydride elimination operates towards coordination site 1, the PNP ligand will stay at bent geometry. Because the agostic effect will activate the C-H bond, **I-TS6$_{bent}$** will proceed a lower energy barrier ($\Delta G^{\ddagger}$ = 23.4 kcal/mol) compared with **cis-I-TS6**. After the β-elimination, the acetone will dissociate from the intermediate ***cis*-I-5** (5.1 kcal/mol) or ***trans*-I-5** (7.1 kcal/mol). Finally, the catalytic cycle is closed and the hydride complex is regenerated. Key intermediates and transition states of the inner-sphere non-bifunctional mechanism are depicted in Figure 5.

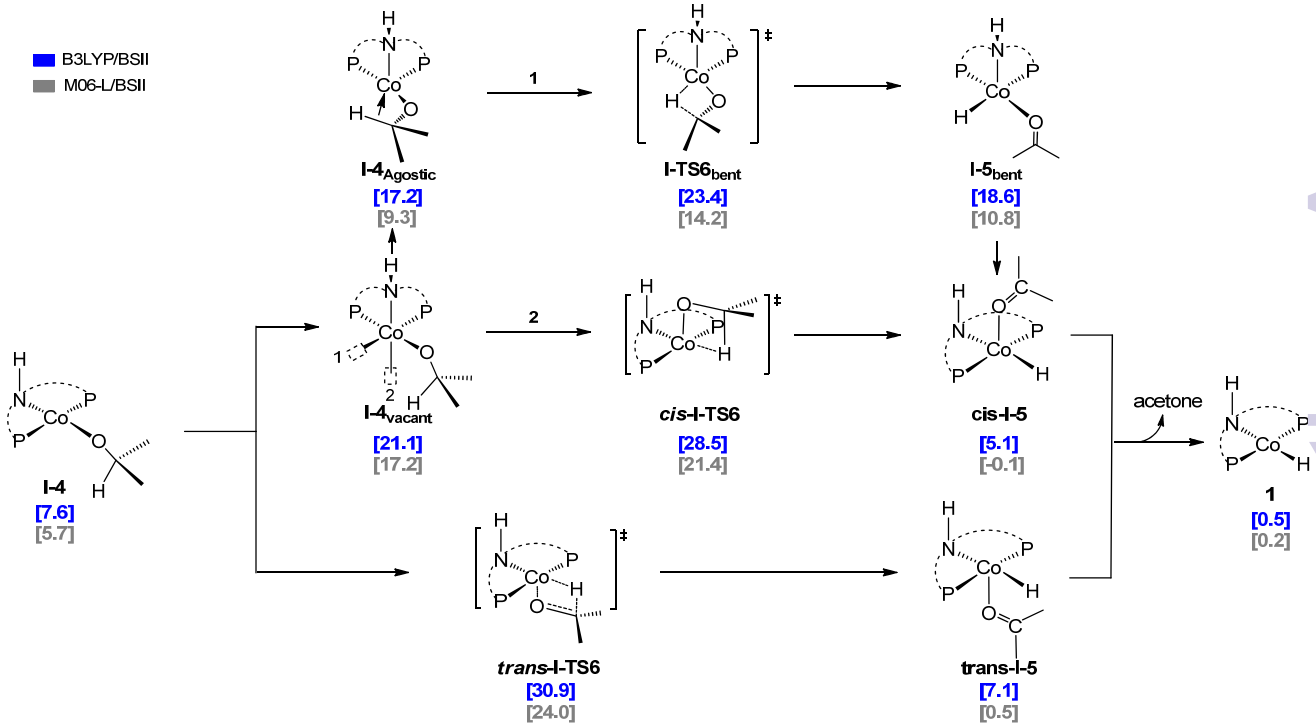

Scheme 4. The β-hydride elimination process of inner-sphere non-bifunctional mechanism. The relative free energies are given in kcal/mol.

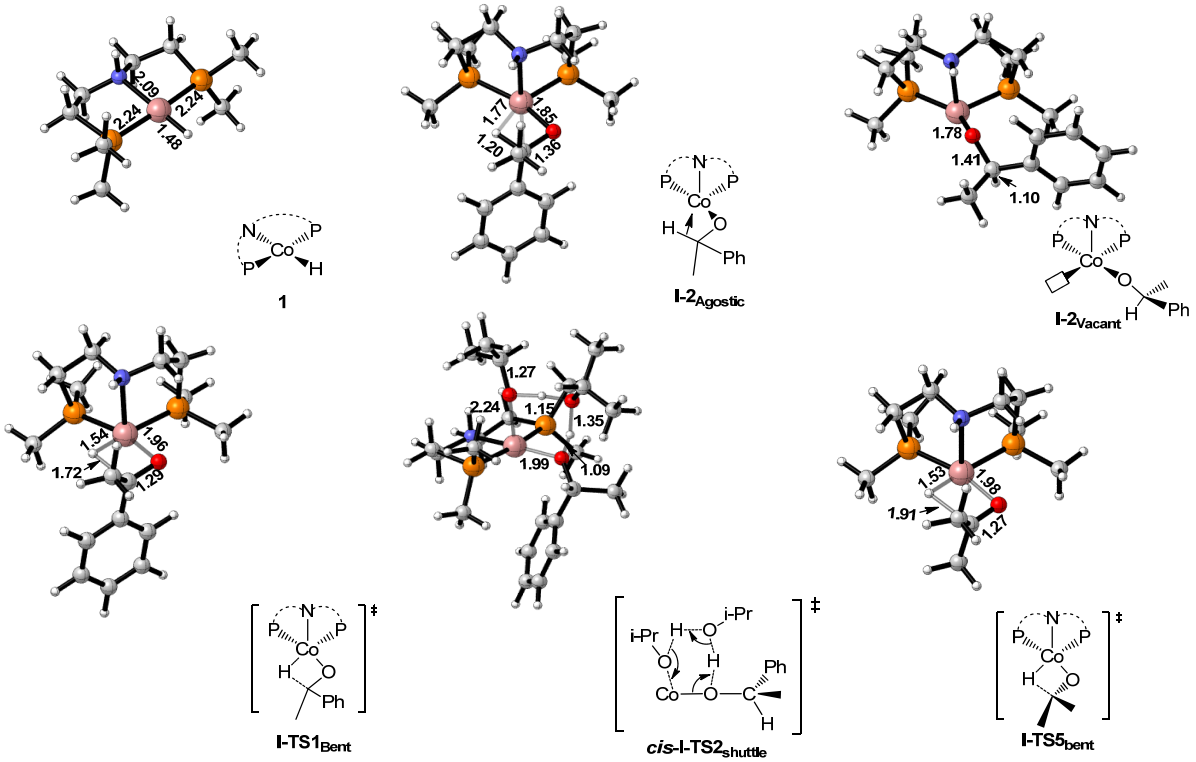

Figure 5. Optimized important intermediates and transition states for non-bifunctional mechanism. Bond lengths are in angstroms.

Outer-sphere concerted transfer hydrogenation. For the outer-sphere mechanism, the substrate AcPh will not interact with the cobalt center. The hydride and the proton of the N-H moiety will transfer to AcPh simultaneously through a six-membered ring transition state to furnish an outer-sphere hydride transfer step. It should be noted that, in order to form this six-membered transition state, the hydride should be nearly perpendicular to the square plane. Only in this way will the $CoH^{\sigma+}$-$NH^{\sigma-}$ moiety interact with AcPh simultaneously, which is essential in other bifunctional catalysts shown in Figure 2. However, the ground state of the starting point **1** stays at a square planar geometry due to the d^7 cobalt center (see Figure 6 A). Therefore, three scenarios are proposed to flip the hydride to the cis site of N-H moiety. One possible way is that when the hydride deforms into the vertical position out of the square plane, the left vacant site is coordinated by an extra ligand. Either the solvent (THF) molecule or the substrate, AcPh or IPA (isopropanol) can serve as an extra ligand to coordinate to the metal center, help-

ing it to transfer into a square-based pyramidal geometry (Figure 6 B). Thus, the hydride and N-H moiety are in proper *cis* positions for bifunctional hydrogenation. The six-coordinated species are also evaluated. The six-coordinated Co^{II} species are excluded due to the unreasonable 19e electronic configuration. As for the six-coordinated Co^{III} species, both calculations and experimental observation[51] suggest the species are less feasible as compared to Co^{II} promoted non-bifunctional mechanism (please see page S8 in Supporting Information, Figure S6).

Besides, the bifunctional transfer via the isomer complex bearing a bent PNP backbone ("butterfly" type: Figure 6 C) is also taken into our consideration. The transition state via the "butterfly" type complex is very high ($\Delta G^{\ddagger}$ = 48.4 kcal/mol) (please see page S6 in Supporting Information, Figure S4). Another possible way is to excite the d^7 complex from doublet to quartet. Then, the quartet complex will be able to undergo the hydride transfer with a tetrahedral geometry via an outer-sphere six-membered ring transition state (Figure 6 D). However, the free energy penalty of the quartet intermediate (**O-1$_{quartet}$**) is 10.2 kcal/mol (12.1 kcal/mol for enthalpy). This quartet six-membered ring TS (**O-TS1$_{quartet}$**) is very high ($\Delta G^{\ddagger}$ = 41.2 kcal/mol) compared with other pathways (please see page S6 in Supporting Information, Figure S3). Therefore, this assumption based on the quartet intermediate is not reasonable as the Co^{II} center intends to stay at a low-spin status. Since then, we rule out these two pathways. Following discussion will focus on the more plausible ground state (doublet), square-based pyramidal geometry (Figure 6 B).

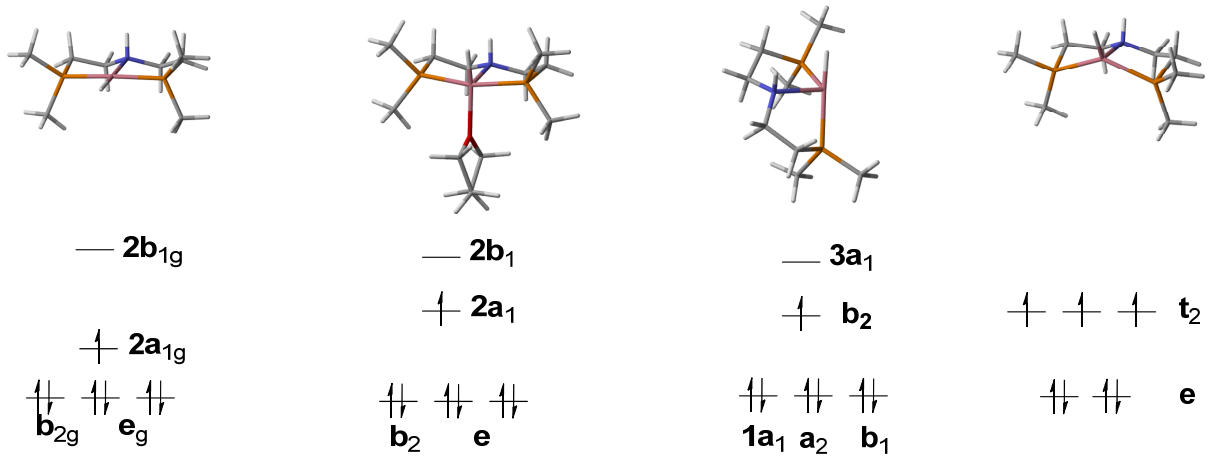

Figure 6. The comparison of different coordination geometries and their electronic configurations of the metal center.

The outer-sphere mechanism can be divided into two steps, the transfer hydrogenation and hydride regeneration step. In the first step, the substrate, AcPh will be hydrogenated through a metal-ligand co-operation process. In the second step, the metal hydride will be regenerated with the hydrogen source (IPA). This process also undergo an outer-sphere bifunctional mechanism. The calculated result of the outer-sphere bifunctional transfer are summarized and compared in Scheme 5. In the case of the catalytic pathways using extra ligand, the catalytic cycle begins with the coordination of IPA, AcPh or THF. From the free energy profile, we can see both of the three coordination situation are uphill (14.5 kcal/mol, 10.2 kcal/mol and 8.4 kcal/mol for IPA, AcPh and THF, respectively). This is mainly due to the entropy penalty and distortion energy caused by the change of ligand field. However, this synchronous transfer hydrogenation has rather high activation free energy ($\Delta G^{\ddagger}$ = 44.4 kcal/mol, 42.6 kcal/mol and 39.4 kcal/mol for **O-TS1$_{IPA}$**, **O-TS1$_{AcPh}$** and **O-TS1$_{THF}$**, respectively). During the hydride transfer, as the Co-H bond is nearly broken, the complex will reform to the four-coordinated square planar geometry. Therefore, the extra ligand of **O-TS1$_{IPA}$**, **O-TS1$_{AcPh}$** and **O-TS1$_{THF}$** seem to be on the same plane of PNP ligand. After the bifunctional transfer, these transition states will lead to d^7 doublet four-coordinated intermediates, **O-3$_{IPA}$**, **O-3$_{AcPh}$** and **O-3$_{THF}$**, which are thermodynamically uphill (16.9

kcal/mol, 13.5 kcal/mol and 11.2 kcal/mol for IPA, AcPh and THF, respectively). During the second process, the hydrogen source, IPA, will react with the **O-3** to regenerate the catalyst via an outer-sphere transition state, **O-TS2$_{IPA}$** ($\Delta G^{\ddagger}$ = 44.2 kcal/mol)**,** **O-TS2$_{AcPh}$** ($\Delta G^{\ddagger}$ = 42.4 kcal/mol) or **O-TS2$_{THF}$** ($\Delta G^{\ddagger}$ = 39.2 kcal/mol). The bifunctional outer-sphere catalytic cycle closes after the dissociation of the ligand and the catalyst **1** is regenerated.

Another outer-sphere mechanism through an eight-member ring is also located, in which an extra IPA molecular will participate the proton transfer process. From Figure 7, we can see that the hydride of the transition state (**O-TS1$_{shuttle}$**) stays at the square planar geometry. However, the ring strain and steric repulsion caused by this loose eight-member ring transition state result in a much higher activation free energy ($\Delta G^{\ddagger}$ = 55.7 kcal/mol for **O-TS1$_{shuttle}$** and $\Delta G^{\ddagger}$ = 55.4 kcal/mol for **O-TS2$_{shuttle}$**, respectively). Moreover, this mechanism is also disfavored due to the entropy penalty. The relative free energy of the highly active amido intermediate **O-3** is 24.8 kcal/mol. Therefore, this transfer mode is considered to be less plausible and can be ruled out.

From the overall PES of outer-sphere mechanism, the coordination situation IPA and AcPh are slightly higher than that of THF. IPA and AcPh are bulky ligands, which will cause more steric effects. On the other hand, the difference in trans-effect leads to a different activation free energy. The overall rate-determining step of the bifunctional transfer hydrogenation proceed through **O-TS1$_{THF}$** with the activation free energy of 39.4 kcal/mol, which is ~12 kcal/mol higher than the rate-determining step of inner-sphere mechanism (***cis*-I-TS2 $_{shuttle}$**: $\Delta G^{\ddagger}$ = 27.6 kcal/mol). Therefore, the calculation results suggest that the non-bifunctional inner-sphere mechanism is more favored in this system. Focusing on the origin of this mechanistic preference, a detailed discussion will be presented in the next section.

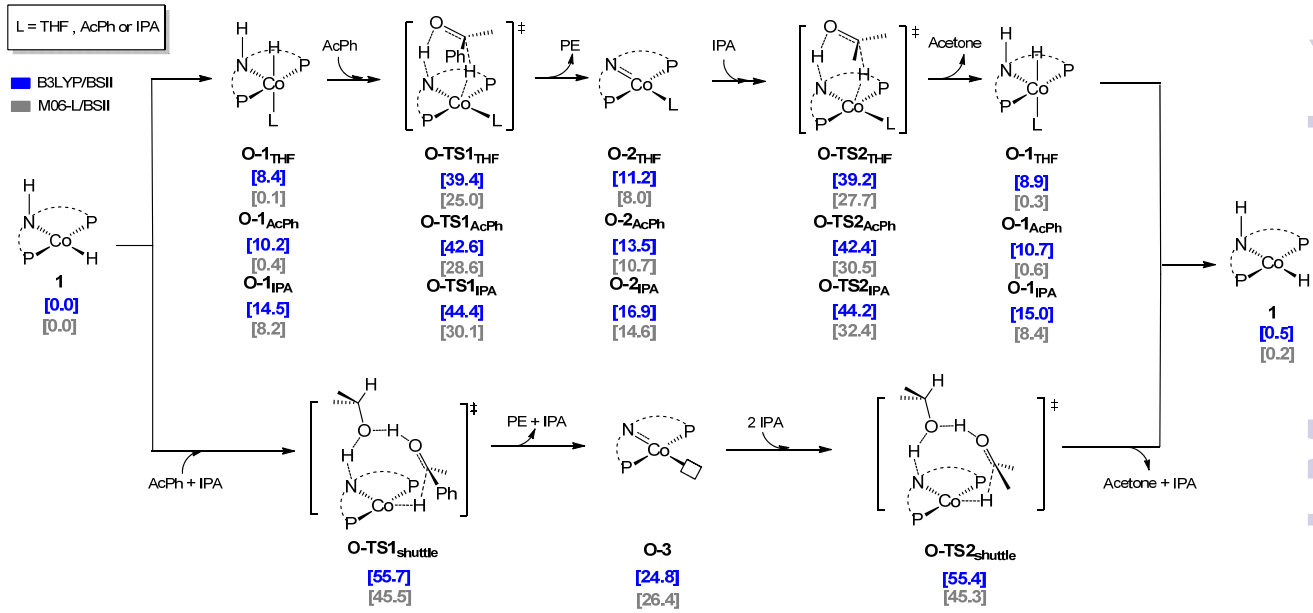

Scheme 5. The outer-sphere bifunctional transfer hydrogenation mechanism. The relative free energies are given in kcal/mol.

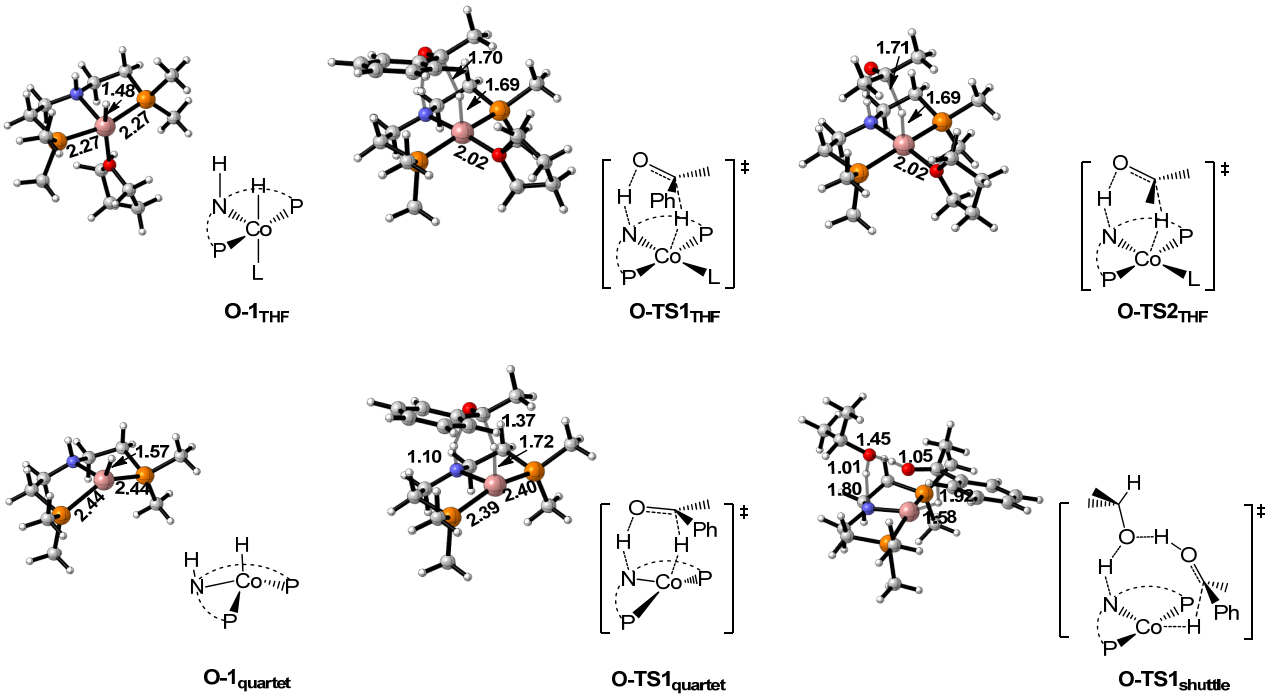

Figure 7. Optimized important intermediates and transition states for bifunctional mechanism. Bond lengths are in angstroms.

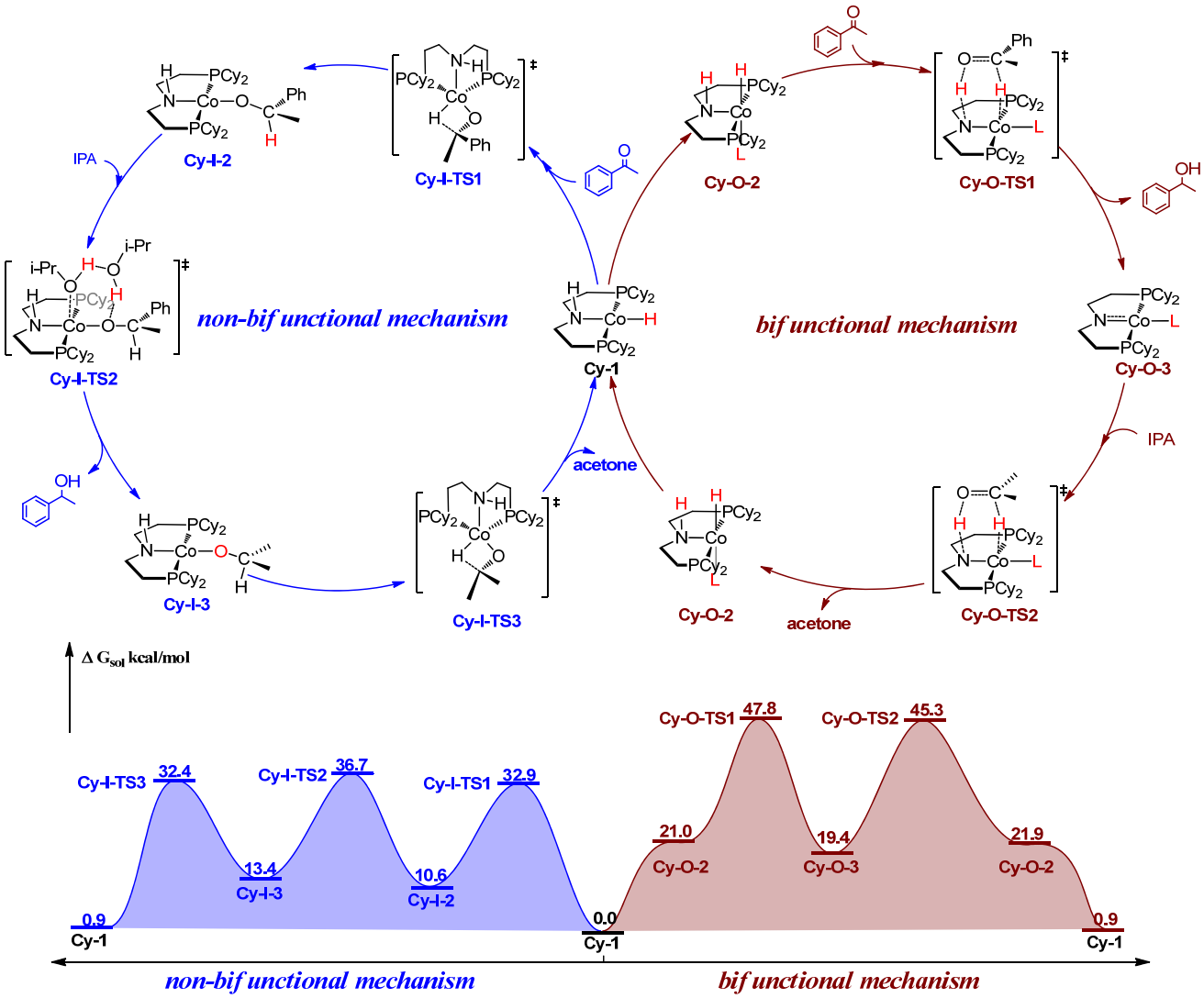

Scheme 6. The overall comparison of non-bifunctional mechanism and bifunctional mechanism for Co-PNP catalyzed transfer hydrogenation based on the full model catalyst. The relative free energies are given in kcal/mol.

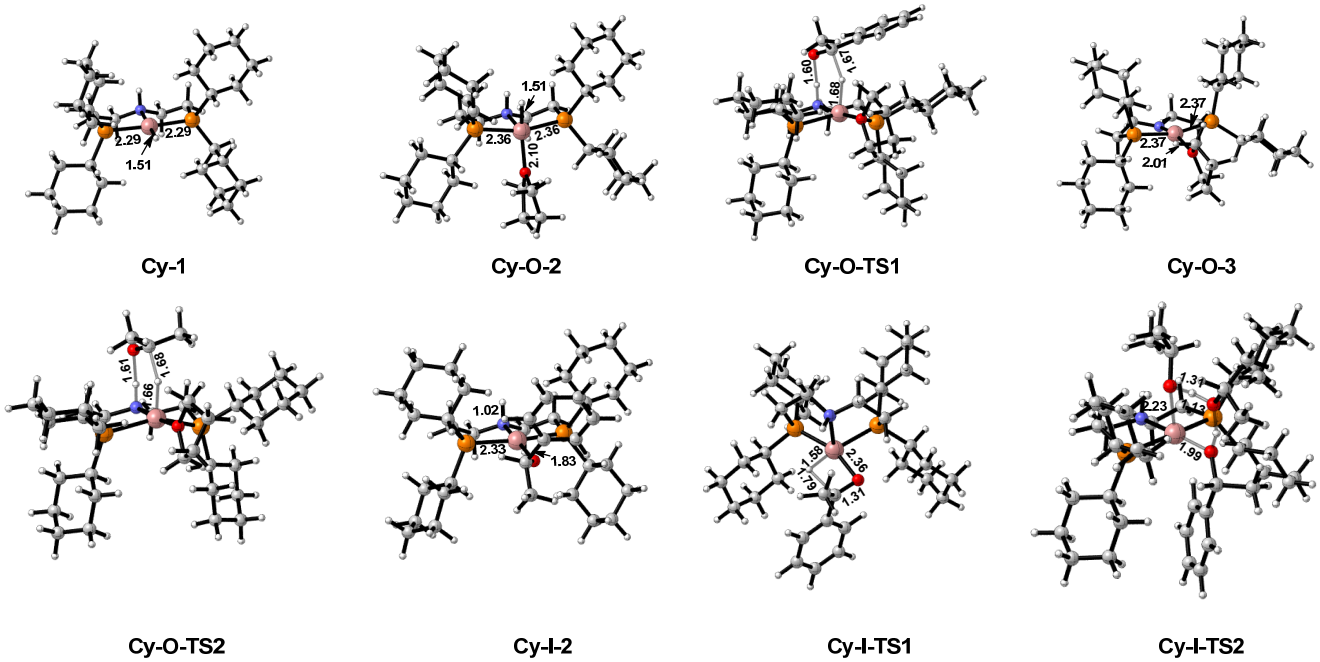

Figure 8. Optimized important intermediates and transition states for bifunctional mechanism based on the full model. Bond lengths are in angstroms.

DISCUSSION

Comparison of two catalytic cycles and the origin of the mechanism preference. With the understanding of different pathways, we then analyze the favorite mechanism and the origin of mechanistic preference for transfer hydrogenation of ketone catalyzed by the Co-PNP complex. Due to the steric effect of the cyclohexane ligand is different from methyl, we performed a full model calculation based on our former calculated results. The overall comparison based on full model of bifunctional mechanism and non-bifunctional mechanism are summarized in Scheme 6. The final calculated results is refined with M06L functional, which is considered to give accurate results in organometallic thermochemistry. The comparison among different functionals are summarized in Supporting Information (page S13). The optimized structures are shown in Figure 8. From the results, we can see the steric effect of cyclohexane is obvious compared with the original result. The reaction free energy increased by ~10 kcal/mol for each intermediates and transition states compared with simple model. However, it did not change the trend of mechanistic preference. The rate-determining step (**Cy-O-TS1**) of outer-sphere mechanism in-

creases to 47.8 kcal/mol, which is ~11 kcal/mol higher than the rate-determining step of (**Cy-I-TS2**: $\Delta G^{\neq}$ = 36.7 kcal/mol). Despite the large differences in barrier heights between the two calculation methods, the results based on the full model at the M06-L/BSII level are qualitatively consistent with B3LYP/BSII results (please see Supporting Information, Figure S7). Using isotope labeling experiments, Hanson et al also verified the mechanism to be monohydride mechanism, which means the hydride from the hydrogen donor ends up as a C–H in the product. Therefore, our calculation result is in good agreement with the experimental observation by Hanson et al. that the PNP ligand is innocent in this system.

A question naturally arises, how do we rationalize this phenomenon? As we can see from Scheme 6, although the non-bifunctional mechanism occurs stepwise, it overcomes much lower energy barrier. For two mechanisms, they will both proceed the coordination process to a five-coordinated complex. The energy increase is similar to each other. However, the inner sphere mechanism will have some advantage in bond breaking and formation process. The advantage of non-bifunctional mechanism via inner sphere is reflected in the three major step of transfer hydrogenation. For the hydride transfer step, the metal center will have an induction effect. Compared with the N-H moiety, the induction effect of Co^{II} center is much stronger. The carbon atom of acetophenone will become more electrophilic due to the induction effect and then facilitate the hydride transfer. Secondly, for the proton transfer step via non-bifunctional mechanism, the proton coming from IPA is easier to transfer compared with N-H moiety due to the lower pK_a of IPA. The metal center also plays important role in facilitate O-H bond breaking in this step. As for the catalyst regeneration step, the non-bifunctional mechanism proceeds via the β-hydride elimination on the inner sphere. The complex will form an agostic bond firstly, which can be viewed as a activation process, as the bond length of C-H is clearly stretched (~0.1 Å). However, the bifunctional manner in the outer-sphere does not have the agostic effect to activate the C-H bond, which leads to a much higher energy barrier to regenerate the catalyst. Therefore, the Co^{II}-PNP chose to proceed inner sphere non-bifunctional mechanism.

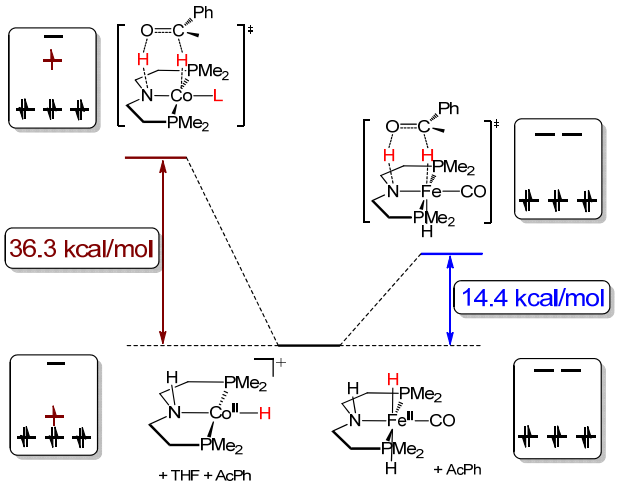

Figure 9. The comparison of deformation energies between non-bifunctional Co-PNP catalyst and bi-functional Fe-PNP catalyst.

Comparison of Fe-PNP catalyst and Co-PNP catalyst. A clear contrast to this Co-PNP system is the Fe-PNP catalytic hydrogenation system developed by Beller et al[52] and Guan et al[57], separately, which has been verified to proceed an outer-sphere bifunctional mechanism. Although these two catalysts bear almost the same pincer back-bone, the d^6 Fe center tends to maintain an octahedral geometry during the catalysis process, wherein the hydride and N-H moiety are *cis* to each other. We calculated the activation free energy of outer-sphere bifunctional mechanism and inner-sphere non-bifunctional mechanism for Fe-PNP catalyst (see page S3 in Supporting Information) based on the simplified model. The bifunctional pathway of Fe-PNP catalyst has the lowest activation free energy ($\Delta G^{\ddagger}$ = 21.9 kcal/mol) compared with other inner-sphere pathways. The activation strain mode analysis is preformed to compare the Fe-PNP catalyst and the Co-PNP catalyst. The comparison results are summarized in Figure 10. The deformation energy of Fe-PNP catalyst is not increased significantly (14.4 kcal/mol) when forming the bifunctional-type transition state. In a sharp contrast, the deformation energy of Co-PNP catalyst increases by 36.3 kcal/mol when the electron structure changes from square planar ligand field to a square-based pyramidal ligand field. These difference in deformation energy is attributed to that there's a singly occupied antibonding orbital on the Co d^7 center. On the other hand, the π-acidic ligand, carbonyl compound, helps the Fe center staying at a low spin status and stabilizes the PNP complex by

the back-donation effect. Therefore, although these two catalysts bear the same pincer backbone which all have the ancillary N-H moiety, the preference of hydrogenation mechanism is truly relied on the electronic configuration of the metal center.

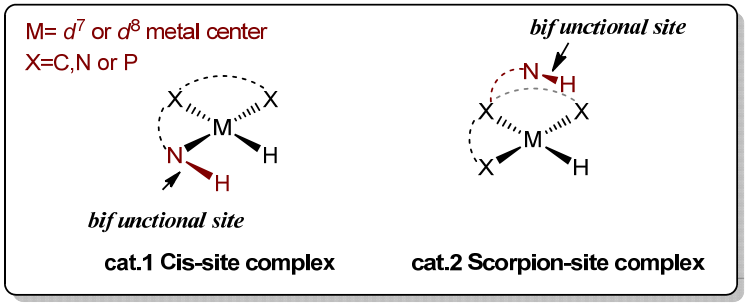

Figure 10. Two proposed bifunctional pincer catalysts with d^7 or d^8 mental center.

For future catalyst design using Co^{II}, Ni^{II} or any other metal centers with d^7 or d^8 electronic configuration, there are two possible strategies to perform bifunctional hydrogenation. The N-H moiety can be attached on the cis-position of metal hydride to avoid the extra deformation energy (Figure 10, cat.1), which may offer a chance for bifunctional transfer hydrogenation. The scorpion-type complex (Figure 10, cat.2) can also be a potential candidate for avoiding the disfavored deformation energy.

CONCLUSION

In summary, a computational study is performed to illuminate the mechanism of the Co^{II}-PNP catalyzed transfer hydrogenation. Using a simplified model complex, we evaluate both inner-sphere and outer-sphere mechanisms. Our calculation indicates that the mechanism will proceed through the inner-sphere non-bifunctional mechanism. The outer-sphere bifunctional mechanism has a higher activation free energy (> ~11 kcal/mol), which is in good agreement of the experimental observation that metal-ligand cooperation is not essential in this system. An overall comparison of both inner-sphere and outer-sphere mechanisms suggests that the preference of the non-bifunctional mechanism can be attributed to the high deformation energy of the catalyst caused by ligand field change during bifunctional process. To verify our assumption, a similar Fe^{II}-PNP catalyst is discussed, which prefers the bifunctional

mechanism. As compared to Co^{II}-PNP system, Fe^{II}-PNP requires high energy penalty to proceed inner sphere mechanism because it tends to maintain the 18e octahedral geometry with the aid of pincer ligands and carbonyl ligand.

Bifunctional catalysis is a popular way to design hydrogenation catalysts through the cooperation of metal and ligand. Our calculations reveal that the catalytic mechanism is not only determined by the structure of the ligand, but also the electronic configuration of the metal center, which will have the decisive impact on the coordination status of the catalyst and then affects the mechanism of the whole catalytic cycle. The spectator ligand, such as pincer ligand and carbonyl ligand, can also affect the mechanistic preference by keep the complex stable. These findings are expected to provide useful guidance of rational catalyst design concerning different electronic configuration of transition metal centers in the future.

COMPUTATIONAL DETAILS

All calculations were performed using Gaussian 09 program.[58] The widely-used B3LYP functional was selected in this study considering the accuracy and computation expense.[59,60] Geometry optimizations were carried out with B3LYP/BSI level (BSI designates the basis set combination of Lanl2DZ[61] for metal atom and 6-31g (d, p) for nonmetal atoms). Frequency analysis calculations were performed to characterize the structures to be the minima (no imaginary frequency) or transition states (one imaginary frequency). Transition states were verified by IRC calculations. At B3LYP/BSI geometries, the free energy results were refined by calculating the single point energy at B3LYP/BSII level with larger basis set (BSII designates Lanl2DZ for metal atom and 6-311++g (d, p) for nonmetal atoms). The bulky solvation effect of THF was simulated by the SMD[62] continuum solvent mode. The cyclohexyl ligand was simplified to methyl for the purpose of reducing the cost of computation. It is generally considered the calculation using ideal gas model will overestimate the entropic contribution due to the ignorance of the suppression effect of solvent on the translation and rotational freedoms of reactants. In order to reduce the overestimation of entropy, a common method is the MHP scheme proposed by Martin, Hay and

Pratt[63]. Based on the theoretical MHP method, Wang et al calculated the correction value to be 4.3 kcal/mol, which can give a reasonable result.[53,55,64,65] Using their approach, an additional 4.3 kcal/mol free energy correction was added to each component (i.e., a reaction from m components to n components, the correction is (n-m) × 4.3 kcal/mol). The final free energy result of the species in the catalytic process was refined with this correction. Therefore, the standard Gibbs free energy of each species is calculated by the equation (1),

$$G^{\circ}_{(sol)} = E^{\circ}_{(gas)} + \Delta G_{solv} + \varepsilon_{ZPE} + G^{\circ}_{298K} + 4.3\ \text{kcal/mol} \quad (1)$$

Where the $E°_{(gas)}$ designates the electronic energy in the gas phase, ΔG_{solv} is the solvation free energy from 1M gas sphere to 1M aqueous sphere. ε_{ZPE} is the gas sphere zero-point energy and the G^{o}_{298K} is the thermal contribution to Gibbs free energy at 298.15K. From the data in the results section, we can see that although the energy barrier is lower for M06-L functional, the predicted mechanistic preference is consistent with the results of B3LYP/BSII/SMD//B3LYP/BSI level. The difference between M06-L and B3LYP can be attributed to the dispersion effect, which are not included in B3LYP functional. At M06-L/BSII level, we checked the relative energy of the rate-determining transition states optimized by different functionals with dispersion effects (B3LYP-D3 and M06-L). The difference in the energy results is quite small for M06-L/BSII/SMD//B3LYP/BSI, M06-L/BSII/SMD//B3LYP-D3/BSI, and M06-L/BSII/SMD//M06-L/BSI (please see page S15 in the Supporting Information). The predicted mechanism is still the same when changing different functional to optimize the structure. But we admit the difference in geometry between B3LYP, B3LYP-D3 and M06-L do exist. Therefore, the results of relative energy based on M06-L/BSII/SMD//B3LYP/BSI level calculation are shown as a comparison with B3LYP/BSII/SMD//B3LYP/BSI data.[66] The main discussion of the mechanistic preference will be based on the results of B3LYP/BSII/SMD//B3LYP/BSI level. The 3D optimized structure figures in this paper were displayed by CYLview visualization program.[67]

ACKNOWLEDGMENT

This work was supported by the NSFC funding (Grants 21203256, 21473261, 21173273, and 21373277). Computing facilities were supported in part by the high performance grid computing platform of Sun Yat-sen University, the Guangdong Province Key Laboratory of Computational Science, and the Guangdong Province Computational Science Innovative Research Team.

REFERENCES

1 Johnson, N. B.; Lennon, I. C.; Moran, P. H.; Ramsden, J. A. *Accounts. Chem. Res.* **2007**, *40*, 1291.
2 Darensbourg, M. Y.; Bethel, R. D. *Nat. Chem.* **2012**, *4*, 11.
3 Barton, B. E.; Olsen, M. T.; Rauchfuss, T. B. *Curr. Opin. Biotechnol.* **2010**, *21*, 292.
4 Gloaguen, F.; Rauchfuss, T. B. *Chem. Soc. Rev.* **2009**, *38*, 100.
5 Appel, A. M.; Bercaw, J. E.; Bocarsly, A. B.; Dobbek, H.; DuBois, D. L.; Dupuis, M.; Ferry, J. G.; Fujita, E.; Hille, R.; Kenis, P. J. A.; Kerfeld, C. A.; Morris, R. H.; Peden, C. H. F.; Portis, A. R.; Ragsdale, S. W.; Rauchfuss, T. B.; Reek, J. N. H.; Seefeldt, L. C.; Thauer, R. K.; Waldrop, G. L. *Chem. Rev.* **2013**, *113*, 6621.
6 Crabtree, R. H. *New J. Chem.* **2011**, *35*, 18.
7 Fujita, E.; Muckerman, J. T.; Himeda, Y. *Bba-bioenergetics* **2013**, *1827*, 1031.
8 Ikariya, T.; Blacker, A. J. *Accounts. Chem. Res.* **2007**, *40*, 1300.
9 Clapham, S. E.; Hadzovic, A.; Morris, R. H. *Coordin. Chem. Rev.* **2004**, *248*, 2201.
10 Karvembu, R.; Prabhakaran, R.; Natarajan, K. *Coordin. Chem. Rev.* **2005**, *249*, 911.
11 Menashe, N.; Salant, E.; Shvo, Y. *J. Organomet. Chem.* **1996**, *514*, 97.
12 Menashe, N.; Shvo, Y. *Organometallics.* **1991**, *10*, 3885.
13 Shvo, Y.; Czarkie, D.; Rahamim, Y.; Chodosh, D. F. *J. Am. Chem. Soc.* **1986**, *108*, 7400.
14 Blum, Y.; Czarkie, D.; Rahamim, Y.; Shvo, Y. *Organometallics.* **1985**, *4*, 1459.
15 Noyori, R.; Ohkuma, T. *Angew. Chem. Int. Ed.* **2001**, *40*, 40.
16 Ohkuma, T.; Doucet, H.; Pham, T.; Mikami, K.; Korenaga, T.; Terada, M.; Noyori, R. *J. Am. Chem. Soc.* **1998**, *120*, 1086.
17 Ohkuma, T.; Ooka, H.; Hashiguchi, S.; Ikariya, T.; Noyori, R. *J. Am. Chem. Soc.* **1995**, *117*, 2675.
18 Di Tommaso, D.; French, S. A.; Zanotti-Gerosa, A.; Hancock, F.; Palin, E. J.; Catlow, C. R. A. *Inorg. Chem.* **2008**, *47*, 2674.
19 Leyssens, T.; Peeters, D.; Harvey, J. N. *Organometallics.* **2008**, *27*, 1514.
20 Yamakawa, M.; Ito, H.; Noyori, R. *J. Am. Chem. Soc.* **2000**, *122*, 1466.
21 Xie, J.-B.; Xie, J.-H.; Liu, X.-Y.; Kong, W.-L.; Li, S.; Zhou, Q.-L. *J. Am. Chem. Soc.* **2010**, *132*, 4538.
22 Malacea, R.; Poli, R.; Manoury, E. *Coordin. Chem. Rev.* **2010**, *254*, 729.
23 Le Roux, E.; Malacea, R.; Manoury, E.; Poli, R.; Gonsalvi, L.; Peruzzini, M. *Adv. Synth. Catal.* **2007**, *349*, 309.
24 Pannetier, N.; Sortais, J. B.; Issenhuth, J. T.; Barloy, L.; Sirlin, C.; Holuigue, A.; Lefort, L.; Panella, L.; de Vries, J. G.; Pfeffer, M. *Adv. Synth. Catal.* **2011**, *353*, 2844.
25 Mikami, K.; Wakabayashi, K.; Yusa, Y.; Aikawa, K. *Chem. Commun.* **2006**, 2365.
26 Baratta, W.; Ballico, M.; Esposito, G.; Rigo, P. *Chem.-Eur. J.* **2008**, *14*, 5588.
27 Takehara, J.; Hashiguchi, S.; Fujii, A.; Inoue, S.; Ikariya, T.; Noyori, R. *Chem. Commun.* **1996**, 233.
28 Hashiguchi, S.; Fujii, A.; Takehara, J.; Ikariya, T.; Noyori, R. *J. Am. Chem. Soc.* **1995**, *117*, 7562.
29 Casey, C. P.; Guan, H. *J. Am. Chem. Soc.* **2009**, *131*, 2499.
30 Casey, C. P.; Guan, H. R. *J. Am. Chem. Soc.* **2007**, *129*, 5816.
31 Lu, X.; Zhang, Y. W.; Zhang, M. T.; Li, T. L. *J. Organomet. Chem.* **2014**, *749*, 69.
32 Lu, X.; Zhang, Y. W.; Yun, P.; Zhang, M. T.; Li, T. L. *Org. Bio. Chem.* **2013**, *11*, 5264.

33 Gunanathan, C.; Ben-David, Y.; Milstein, D. *Science* **2007**, *317*, 790.
34 Li, H.; Wang, X.; Huang, F.; Lu, G.; Jiang, J.; Wang, Z.-X. *Organometallics.* **2011**, *30*, 5233.
35 Li, H.; Wang, X.; Wen, M.; Wang, Z.-X. *Eur. J. Inorg. Chem.* **2012**, *2012*, 5011.
36 Yang, X.; Hall, M. B. *J. Am. Chem. Soc.* **2009**, *131*, 10901.
37 Zeng, G.; Li, S. *Inorg. Chem.* **2011**, *50*, 10572.
38 Mikhailine, A. A.; Maishan, M. I.; Morris, R. H. *Org. Lett.* **2012**, *14*, 4638.
39 Mikhailine, A. A.; Maishan, M. I.; Lough, A. J.; Morris, R. H. *J. Am. Chem. Soc.* **2012**, *134*, 12266.
40 Lagaditis, P. O.; Lough, A. J.; Morris, R. H. *J. Am. Chem. Soc.* **2011**, *133*, 9662.
41 Lagaditis, P. O.; Lough, A. J.; Morris, R. H. *Inorg. Chem.* **2010**, *49*, 10057.
42 Mikhailine, A.; Lough, A. J.; Morris, R. H. *J. Am. Chem. Soc.* **2009**, *131*, 1394.
43 Zuo, W.; Tauer, S.; Prokopchuk, D. E.; Morris, R. H. *Organometallics.* **2014**, 5791.
44 Sues, P. E.; Demmans, K. Z.; Morris, R. H. *Dalton. Trans.* **2014**, *43*, 7650.
45 Zuo, W. W.; Lough, A. J.; Li, Y. F.; Morris, R. H. *Science* **2013**, *342*, 1080.
46 Prokopchuk, D. E.; Sonnenberg, J. F.; Meyer, N.; Zimmer-De Iuliis, M.; Lough, A. J.; Morris, R. H. *Organometallics.* **2012**, *31*, 3056.
47 Prokopchuk, D. E.; Morris, R. H. *Organometallics.* **2012**, *31*, 7375.
48 Zhang, G. Q.; Vasudevan, K. V.; Scott, B. L.; Hanson, S. K. *J. Am. Chem. Soc.* **2013**, *135*, 8668.
49 Zhang, G. Q.; Hanson, S. K. *Org. Lett.* **2013**, *15*, 650.
50 Zhang, G. Q.; Scott, B. L.; Hanson, S. K. *Angew. Chem. Int. Ed.* **2012**, *51*, 12102.
51 Zhang, G. Q.; Hanson, S. K. *Chem. Commun.* **2013**, *49*, 10151.
52 Werkmeister, S.; Junge, K.; Wendt, B.; Alberico, E.; Jiao, H.; Baumann, W.; Junge, H.; Gallou, F.; Beller, M. *Angew. Chem. Int. Ed.* **2014**, 8722.
53 Qu, S.; Dai, H.; Dang, Y.; Song, C.; Wang, Z.-X.; Guan, H. *ACS Catalysis* **2014**, *4*, 4377.
54 Chakraborty, S.; Lagaditis, P. O.; Förster, M.; Bielinski, E. A.; Hazari, N.; Holthausen, M. C.; Jones, W. D.; Schneider, S. *ACS Catalysis* **2014**, *4*, 3994.
55 Qu, S.; Dang, Y.; Song, C.; Wen, M.; Huang, K.-W.; Wang, Z.-X. *J. Am. Chem. Soc.* **2014**, *136*, 4974.
56 Qu, S.; Dang, Y.; Wen, M.; Wang, Z.-X. *Chemistry – A European Journal* **2013**, *19*, 3827.
57 Chakraborty, S.; Dai, H.; Bhattacharya, P.; Fairweather, N. T.; Gibson, M. S.; Krause, J. A.; Guan, H. *J. Am. Chem. Soc.* **2014**, *136*, 7869.
58 M. J. G. Frisch **2009**, Gaussian 09.
59 Li, H. X.; Lu, G.; Jiang, J. L.; Huang, F.; Wang, Z. X. *Organometallics.* **2011**, *30*, 2349.
60 Li, H. X.; Jiang, J. L.; Lu, G.; Huang, F.; Wang, Z. X. *Organometallics.* **2011**, *30*, 3131.
61 Hay, P. J.; Wadt, W. R. *J. Chem. Phys.* **1985**, *82*, 299.
62 Marenich, A. V.; Cramer, C. J.; Truhlar, D. G. *J. Phys. Chem. B* **2009**, *113*, 4538.
63 Martin, R. L.; Hay, P. J.; Pratt, L. R. *J. Phys. Chem. A* **1998**, *102*, 3565.
64 Li, H.; Wen, M.; Wang, Z.-X. *Inorg. Chem.* **2012**, *51*, 5716.
65 Wen, M.; Huang, F.; Lu, G.; Wang, Z.-X. *Inorg. Chem.* **2013**, *52*, 12098.
66 Zhao, Y.; Truhlar, D. G. *J. Chem. Phys.* **2006**, *125*, 194101.
67 Legault, C. Y., CYLview, 1.0b; *Université de Sherbrooke* **2009**, http://www.cylview.org.